In vivo characterization of physiological and metabolic changes related to isocitrate dehydrogenase 1 mutation expcression by multiparametric MRI and MRS in a rat model with orthotopically grafted human-derived glioblastoma cell lines

Alexandra Clément, Matthieu Doyen, Florence Fauvelle, Gabriela Hossu, Bailiang Chen, Muriel Barberi-Heyob, Alex Hirtz, Vasile Stupar, Zohra Lamiral, Celso Pouget, et al.

Received: | Accepted: Accepted paper

In vivo characterization of physiological and metabolic changes related to isocitrate dehydrogenase 1 mutation expcression by multiparametric MRI and MRS in a rat model with orthotopically grafted human-derived glioblastoma cell lines

Alexandra Clément[1,2] | Matthieu Doyen[1,2] | Florence Fauvelle[3] | Gabriela Hossu[2,4] | Bailiang Chen[2,4] | Muriel Barberi-Heyob[5] | Alex Hirtz[5] | Vasile Stupar[3] | Zohra Lamiral[6] | Celso Pouget[7] | Guillaume Gauchotte[7] | Gilles Karcher[1,8] | Marine Beaumont[2,4] | Antoine Verger[1,2,8] | Benjamin Lemasson[3]

[1]Nancyclotep Molecular and Experimental Imaging Platform, CHRU Nancy, Nancy, France

[2]Lorraine University, INSERM, IADI UMR 1254, Nancy, France

[3]INSERM, Grenoble University, GIN UMR 1216, Grenoble, France

[4]Lorraine University, CIC-IT UMR 1433, CHRU Nancy, Nancy, France

[5]Lorraine University, CNRS, CRAN UMR 7039, Nancy, France

[6]INSERM, Lorraine University, DCAC UMR 1116, Nancy, France

[7]Department of Pathology, CHRU Nancy, Nancy, France

[8]Department of Nuclear Medicine, CHRU Nancy, Nancy, France

Correspondence
Alexandra Clément, Nancyclotep Molecular and Experimental Imaging Platform, CHRU Nancy, 05 rue du Morvan, 54500 Vandoeuvre-Les-Nancy, France
Email: a.clement@nancyclotep.com

The physiological mechanism induced by the isocitrate dehydrogenase 1 (*IDH1*) mutation, associated with better treatment response in gliomas, remains unknown. The aim of this preclinical study was to characterize the *IDH1* mutation through in vivo multiparametric MRI and MRS. Multiparametric MRI, including the measurement of blood flow, vascularity, oxygenation, permeability, and in vivo MRS, was performed on a 4.7 T animal MRI system in rat brains grafted with human-derived glioblastoma U87 cell lines expressing or not the *IDH1* mutation by the CRISPR/Cas9 method, and secondarily characterized with additional ex vivo HR-MAS and histological analyses. In univariate analyses, compared with IDH1−, IDH1+ tumors exhibited higher vascular density ($p < 0.01$) and better perfusion ($p = 0.02$ for cerebral blood flow), but lower vessel permeability ($p < 0.01$ for time to peak (TTP), $p = 0.04$ for contrast enhancement) and decreased T_1 map values ($p = 0.02$). Using linear discriminant analysis, vascular density and TTP values were found to be independent MRI parameters for characterizing the *IDH1* mutation ($p < 0.01$). In vivo MRS and ex vivo HR-MAS analysis showed lower metabolites of tumor aggressiveness for IDH1+ tumors ($p < 0.01$). Overall, the *IDH1* mutation exhibited a higher vascularity on MRI, a lower permeability, and a less aggressive metabolic profile. These MRI features may prove helpful to better pinpoint the physiological mechanisms induced by this mutation.

KEYWORDS
glioma, *IDH1*, multiparametric MRI, orthotopic, preclinical, spectroscopy

Abbreviations: 2-HG, 2-hydroxyglutarate; BVf, blood volume fraction; CBF, cerebral blood flow; $CMRO_2$, cerebral metabolic rate of oxygen; DCE, dynamic contrast enhanced; GABA, gamma-aminobutyric acid; GLN, glutamine; GLU, glutamate; GSH, glutathione; HR-MAS, high-resolution magic angle spinning spectroscopy; *IDH1*, isocitrate dehydrogenase 1; LDA, linear discriminant analysis; M-INS, myo-inositol; NAA, *N*-acetylaspartate; PCR, phosphocreatine; PRESS, point-resolved spectroscopy; ROI, region of interest; StO_2, tissue oxygen saturation; T_2-w, T_2-weighted; TAU, taurine; T_E, echo time; T_R, repetition time; TTP, time to peak; VSI, vessel size index; WHO, World Health Organization.

Received: | Accepted: Accepted paper

1 | INTRODUCTION

The World Health Organization (WHO) has recently updated the tumor classification of the central nervous system by integrating molecular parameters, and in particular the isocitrate dehydrogenase 1 (*IDH1*) mutation,[1] the expression of which is associated with a better response to chemo- and radiotherapy in gliomas.[2,3]

From a metabolic standpoint, the *IDH1* mutation leads to an intracytoplasmic accumulation of 2-hydroxyglutarate (2-HG) through its reduction from α-ketoglutarate (α-KG), a key component of the Krebs cycle.[4] The accumulation of 2-HG alters the glioma epigenome through increased DNA methylation,[5,6] activates cellular malignant transformation,[7,8] and results in a change in global tumor metabolism by inducing cellular toxicity.[9,10] All of these modifications contribute to the production of reactive oxygen species and induce an increased sensitivity to oxidative damages that may partly explain the better response to treatments observed in *IDH1*-mutant tumors.[2,3,11] The exact mechanisms induced by this metabolite remain nonetheless widely unknown.

The biological events at the molecular, cellular, and tissue levels resulting from the *IDH1* mutation should nevertheless be monitored, preferentially through a non-invasive method, as it can be used as a prognostic biomarker for tumors at initial diagnosis. Among the in vivo techniques, ^{1}H MRS appears to be the most promising tool for the identification of *IDH1* mutant gliomas by highlighting higher levels of 2-HG in these tumors.[12–14] However, this method has demonstrated a relatively high incidence of false positive results, ranging from 18.5% to 26%.[15] Nowadays, a number of structural and functional parameters, such as vascular density, vessel size index (VSI), cerebral blood flow (CBF), blood volume fraction (BVf), tumor oxygenation (tissue oxygen saturation (StO_2)), and cerebral metabolic rate of oxygen ($CMRO_2$), as well as blood-brain barrier integrity (using a dynamic contrast enhanced (DCE) approach with time to peak (TTP) and signal contrast enhancement), are accessible by MRI. Some of these parameters have already been reported to feature other relevant metabolic indicators induced by the *IDH1* mutation.[16] However, a multiparametric MRI approach is likely needed to allow the modifications induced by *IDH1* mutation expression to be established.

Preclinical studies are currently the only means to highlight in a direct manner the features induced by the *IDH1* mutation in vivo, independently of other mutations and tumor characteristics. Previous preclinical studies have attempted to investigate the overexpression of *IDH1* mutation in vivo,[17,18] although, to our knowledge, none with the original objective of specifically studying its pathophysiological expression by inducing such mutation in gliomas with the CRISPR/Cas9 method. This innovative genetic method enables assessment of the sole and basal expression of the *IDH1* mutation.

The aim of this preclinical study was thus to characterize *IDH1* mutation features induced by the expression of this mutation in human-derived U87 glioblastoma cell lines orthotopically implanted into rat brains using in vivo multiparametric MRI and MRS, along with ex vivo high-resolution magic angle spinning spectroscopy (HR-MAS) and histological analysis.

2 | EXPERIMENTAL METHODS

2.1 | Human-derived U87-MG glioblastoma cell lines and validation of the expression of the *IDH1* mutation

Human-derived U87 glioblastoma cell lines, *IDH1*-mutated (IDH1+) and non *IDH1*-mutated (IDH1–), were purchased from the American Type Culture Collection (ATCC, HTB-14IG and HTB-14, Manassas, Virginia, USA). The isogenic IDH1+ cell line was generated from the parental U-87MG (ATCC HTB-14) cell line by the innovative CRIPSR/Cas9 genetic method.[17] This is a heterozygous mutation expressing the c.395G > A mutant allele. Cells were cultured in Dulbecco's modified Eagle minimal essential medium (DMEM) (Gibco, Thermo Fisher, Illkirch-Graffenstaden, France). Growth media were supplemented with 10% fetal bovine serum (FBS) and 100 U/mL penicillin-streptomycin and maintained at 37 °C in an atmosphere of 5% CO_2/95% air.

The validation of *IDH1* mutation expression was performed through Western blot analysis and detection of 2-HG in cells (**Supporting Information**).

2.2 | Animal models

IDH1+ and IDH1– cells were respectively implanted in 11 and 9 athymic male nude rats (200-250 g; RH-Foxn1rnu; Envigo, Gannat, France) as previously described.[18] Briefly, rats were anesthetized with a mixture of air and 1.5-2% isoflurane and placed in a stereotactic frame (900 M Kopf Instruments, Tujunga, California). Thereafter, 5×10^4 human-derived glioblastoma cells, suspended in 5 μL Hank's balanced salt solution (HBSS, ×1), were injected into the right caudate nucleus[19] with the needle of a 10 μL Hamilton syringe.

At the end of the experimental study period, anesthetized animals were sacrificed by decapitation after completion of MRI scans. Available tumor samples were used for ex vivo HR-MAS acquisitions (N = 8 IDH1+ and N = 7 IDH1–) and only the remaining portions of these tumors were used for histological analyses (N = 4 IDH1+ and N = 4 IDH1–).

All protocols were approved by Lorraine Ethics Committee 66 according to Guidelines of Animal Care and Use (APAFIS no. 14056-2,018,031,316,365,081). A schematic diagram of the experimental design is presented in Figure 1A.

2.3 | In vivo MRI and in vivo MRS

2.3.1 | Data acquisition and MRI processing

MRI was performed using a horizontal bore 4.7 T BioSpec animal scanner (Bruker BioSpin, Ettlingen, Germany, Avance III console, Paravision 5.0.1) with a volume/surface cross-coil configuration. Anatomical imaging was first performed on all rats on Day 14 post-graft with a T_2-weighted (T_2-w) image to assess tumor volume, which was used to determine the running order of rats imaged by MRI and MRS (from the largest to the smallest) in order to minimize tumor size variations between IDH1+ (N = 11) and IDH1− (N = 9) groups.[20] The multiparametric MR protocol was applied once for each rat and involved acquired data (raw data), after which derived maps were computed (ie T_2-w, T_1 and T_2 maps, vascular density, VSI, CBF, BVf, $CMRO_2$, StO_2, TTP, percentage of signal enhancement) as presented in Figure 1A.

Overall acquisition time was 90 min. Spatial resolution of all parametric maps was defined from low-resolution graphic maps, ie CBF, VSI, and vascular density maps. Details of sequence acquisitions and MRI processing are described in **Supporting Information**.

A region of interest (ROI) was manually delineated on the T_2-w images of each rat brain on the section with the most extensive tumor region. An additional peripheral tumor ROI was placed automatically 2 pixels outside the surrounding tumor delineation. For healthy tissue, an ROI similar to those applied for the tumor was positioned on the contralateral striatum. Examples of MRI maps and applied ROIs are provided in Figure 1B.

All MRI analyses, including cluster model, were performed using Medical software for Processing multi-Parametric images Pipelines (MP^3) (https://github.com/nifm-gin/MP3).

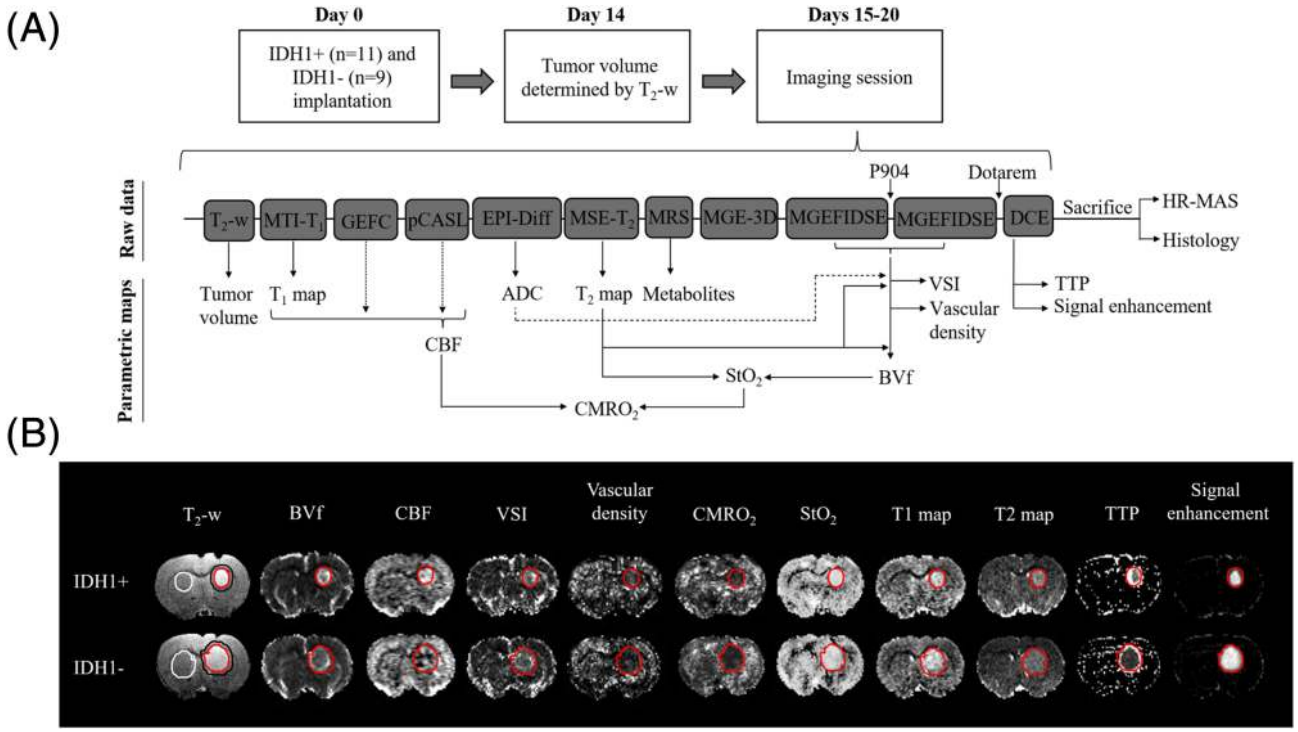

FIGURE 1 A, Flowchart depicting the experimental design. Twenty rats were orthotopically implanted with human-derived U87 cell lines including 11 with the *IDH1*-mutant line. Fifteen days later, the order of animal scans was determined using T_2-w imaging according to tumor volume. The MRI session involved measurement of 11 MRI parameters, namely T_2-w, T_1 and T_2 maps, vascular density, VSI, CBF, BVf, $CMRO_2$, StO_2, TTP and the percentage of signal enhancement, as well as one MRS sequence. B, Representative maps of MRI parameters for IDH1+ and IDH1− tumors. In addition to anatomical T_2-w images, 10 MRI parameters were mapped. On the anatomical T_2-w, the red circle indicates the tumor ROI, the white circle indicates the healthy tissue ROI, and the black circle indicates the delineation of the peripheral tumor area ROI

2.3.2 | Data acquisition and in vivo MRS processing

Spectra were acquired with a short echo time point-resolved spectroscopy (PRESS) sequence,[21] with T_R/T_E = 2500/20 ms, 2203 Hz bandwidth centered on the water frequency, 2048 data points, and 400 moving averages. The total acquisition time was 16 min 40 s. Of note, in vivo MRS acquisition was carried out in the middle of the MR protocol prior to injection of the first contrast agent so as not to interfere with the quantification of metabolites as described in the workflow depicted in Figure 1A. The volume of interest was set at 27 mm^3 ($3 \times 3 \times 3$ mm) and placed in the center of the tumor based on the T_2-w images. The PRESS localization was preceded by the variable power and optimized relaxation delays (VAPOR)[22] water suppression scheme and outer volume suppression modules. The MAPSHIM algorithm[23] was used to optimize the static B_0 field homogeneity within the volume of interest.

Quantification of the in vivo proton MR spectra is described in **Supporting Information**.

2.4 | Ex vivo HR-MAS

Frozen tumor samples were introduced into a cold 4 mm zirconium rotor to which 30 μL of D_2O were added.[24] All HR-MAS NMR spectra were recorded on a Bruker Avance III 500 spectrometer operating at a proton frequency of 500 MHz. Details regarding acquisition and ex vivo HR-MAS processing are described in **Supporting Information**.

2.5 | Histology

Tumor samples were fixed in 4% paraformaldehyde. Paraffin sections 5 μm thick were incubated with the following primary antibodies: Ki-67 (1:200; MIB1, Dako, Les Ulis, France) and anti-IDH1 R132H (1:70, DIA-H09, dianova, Hamburg, Germany), along Dako Autostainer Plus (Dako) and Flex+.[25] Other sections were used for anti-CD31 (1:250, [EPR17259] ab182981, Abcam, Paris, France). All sections were reviewed by two observers (C.P. and A.C.) with an Olympus BX 51 microscope, and quantitative analysis was performed with the ImageJ image-processing software (Version 1.48). *IDH1* expression was assessed in a binary manner: positive or negative marker.

2.6 | Statistical analysis

All analyses were performed using SAS Version 9.4 (SAS Institute, Cary, North Carolina) and R Version 3.6.1. The two-tailed significance level was set at $p < 0.05$ with correction for multiple comparisons. Characteristics of both tumor cell line groups are described as means and standard deviations.

Due to the non-normality of the variables, characteristics of the IDH1 tumor groups were compared using Mann-Whitney or Kruskal-Wallis tests in instances of multiple group comparisons. Paired tests were performed when needed.

For extraction of quantitative MRI parameters, Wilks's lambda test was first used to determine which variable significantly contributed to the separation between the IDH1+ and IDH1− groups, independent of glioblastoma volume. A subset of previously selected variables was finally introduced in the multivariable linear discriminant analysis (LDA). Unsupervised model-based clustering analysis was performed on MRI maps including the aforementioned variable parameters. Voxels in the tumor ROI were clustered using the *K*-means method (squared Euclidean distance metric), and the optimal number of clusters was determined using the slope heuristic method.[26]

3 | RESULTS

3.1 | Confirmation of expression and activity of the *IDH1* mutation in the U87 *IDH1*-mutated cell lines

Expression of the *IDH1* mutation in IDH1+ cell lines was validated by western blotting including GAPDH expression control (Supporting Information Figure S1a), and by immunohistochemistry (Supporting Information Figure S1b). The activity of this mutation was confirmed by a 2.25 times higher intracellular 2-HG concentration in IDH1+ compared with IDH1− cell lines (0.09 ± 0.03 and 0.04 ± 0.01 mM respectively, $p = 0.04$, Supporting Information Figure S1c).

3.2 | MRI characteristics of the *IDH1* mutation

Results of the univariate analysis are detailed in Supporting Information Table S1 and illustrated in Figure 2.

Received: | Accepted: Accepted paper

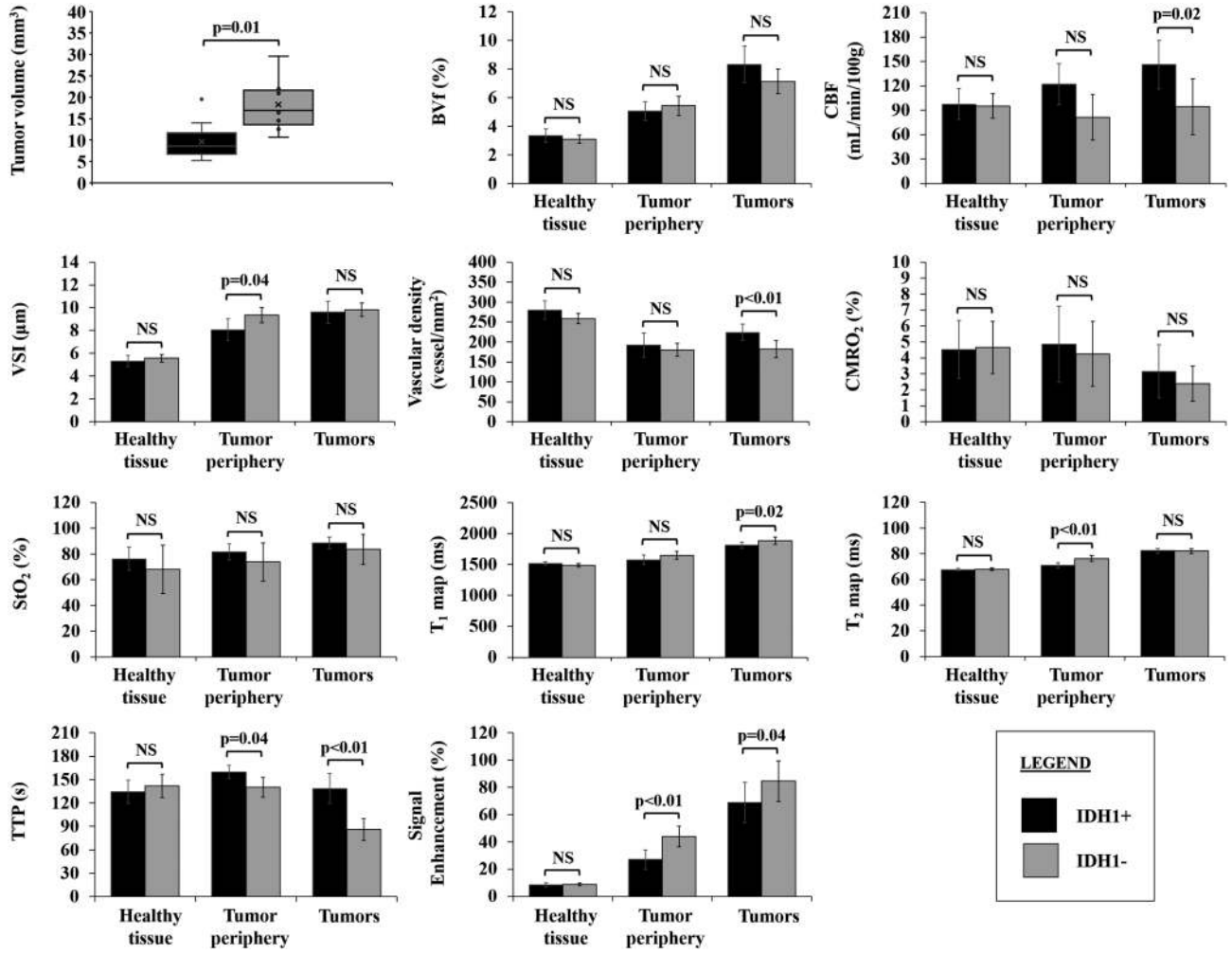

FIGURE 2 Histograms representative of univariate quantitative analysis of MRI parameters for IDH1+ and IDH1− human-derived glioblastomas, tumor periphery areas, and contralateral healthy tissue

In univariate analysis, compared with IDH1− tumors, IDH1+ tumors exhibited lower tumor volume (9.63 ± 4.11 versus 18.30 ± 5.76 mm^3, $p = 0.01$) and lower T_1 values (4.03% decrease, $p = 0.02$), as well as higher values for vascular density (223.78 ± 20.80 versus 181.86 ± 21.23 vessels/mm^2, $p < 0.01$) and CBF (145.92 ± 29.82 versus 94.21 ± 34.58 mL/min/100 g, $p = 0.02$). With regard to vessel permeability, illustrated in Supporting Information Figure S2, IDH1+ tumors were characterized by a longer TTP (138.60 ± 19.20 versus 85.95 ± 13.96 s, $p < 0.01$) as well as a significantly lower contrast enhancement (68.76 ± 14.68 versus 84.43 ± 14.89%, $p = 0.04$). BVf, VSI, $CMRO_2$, StO_2, and T_2 values did not show any significant difference between tumor types ($p > 0.14$).

Peripheral tumor areas exhibited the same characteristics as observed in the tumors. Although IDH1+ tumors showed a reduced VSI (8.07 ± 0.95 versus 9.34 ± 0.67 µm for IDH1− tumors, $p = 0.04$) and T_2 value (71.01 ± 2.06 versus 76.30 ± 2.34 ms for IDH1− tumors, $p < 0.01$), no difference was observed for vessel density ($p = 0.24$), CBF ($p = 0.06$) or T_1 values ($p = 0.06$).

Compared with contralateral normal brain, both tumor types exhibited a lower vessel density as well as higher BVf, CBF, VSI, StO_2, T_1, and T_2 values and contrast enhancement ($p < 0.05$). No difference was observed for $CMRO_2$ or TTP in the IDH1+ tumors ($p > 0.05$), whereas there was a decrease in these parameters for IDH1− tumors compared with the contralateral normal brain ($p < 0.05$).

LDA was performed to identify key features of the *IDH1* mutation. Two quantitative MR parameters were found to be statistically independent of tumor volume, namely vascular density and TTP. Figure 3A shows a clear separation of the two tumor types between these two MR characteristics. A model-based clustering analysis was also performed at the voxel level in order to illustrate voxels sharing the same MRI features according to these two parameters, the latter of which are depicted in Figure 3B and Figure 3C.

Received: | Accepted: Accepted paper

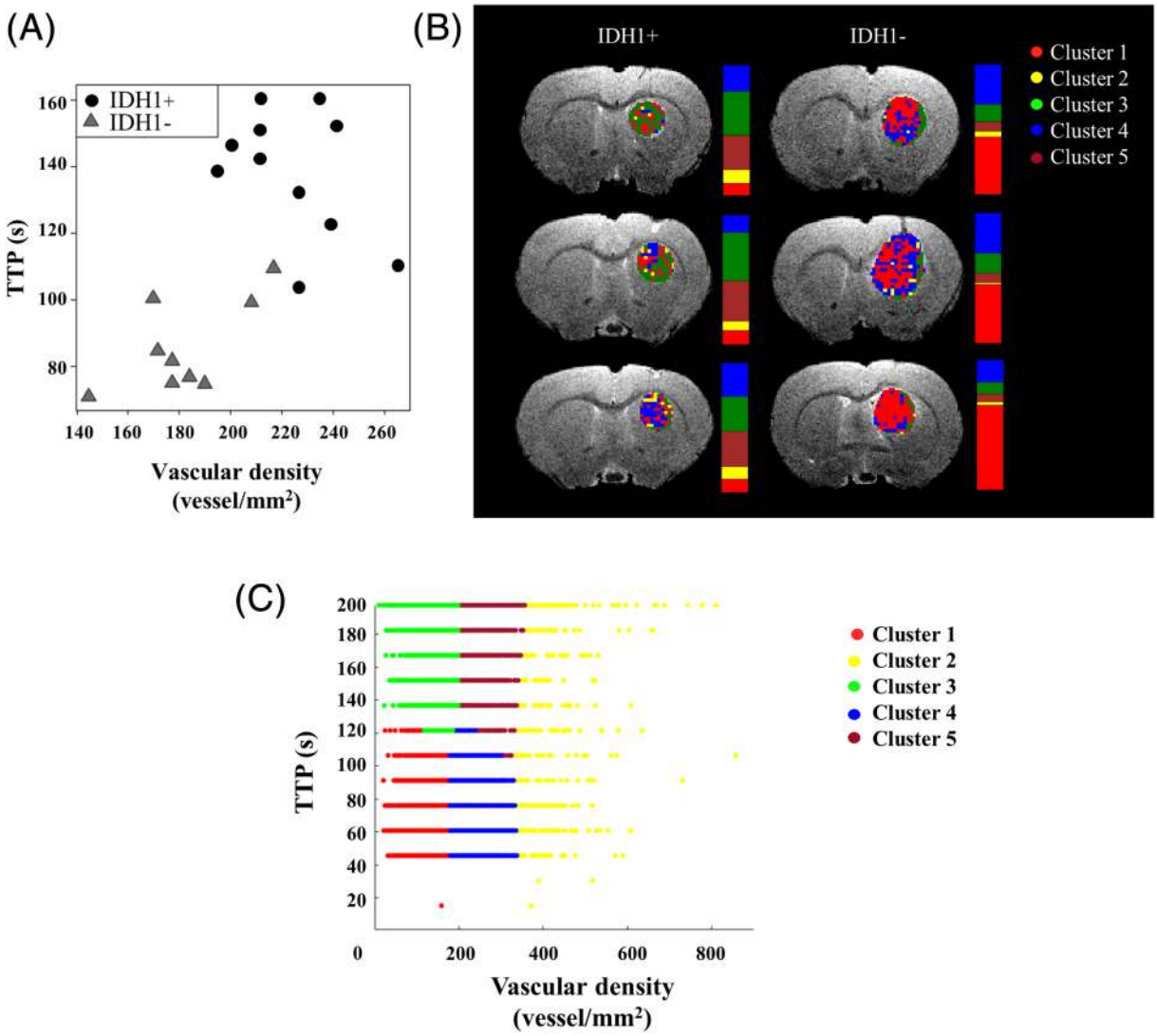

FIGURE 3 A, Graphic representation of the discrimination of *IDH1* mutation in human-derived glioblastomas according to the two independent MR parameters identified by LDA: vascular density and TTP. B, Cluster distribution for vascular density and TTP of IDH1+ and IDH1− tumors. The IDH1+ tumors were represented by a majority of Clusters 3 and 4. By contrast, the IDH1− tumors were represented by Cluster 1. The colored bars illustrate the cluster proportions by percentage within the ROI for the two tumor types in three separate examples. C, Representation of the distribution of all tumor voxels according to TTP and vascular density for each cluster

3.3 | *IDH1* mutation metabolic profiles with in vivo MRS and ex vivo HR-MAS

In vivo and ex vivo proton MR spectra of IDH1− and IDH1+ tumors and results of the quantification of detected metabolites are presented in Figure 4 and Table 1, together with the complete metabolite basis set reported in Table S2 (Supporting Information). Results were consistent between in vivo MRS (Figure 4A) and ex vivo HR-MAS (Figure 4B) methods. In brief, IDH1+ tumors exhibited significant increased concentrations of *N*-acetylaspartate (NAA), phosphocreatine (PCR), taurine (TAU) and myo-inositol (M-INS) and a decreased concentration of glutathione (GSH) in comparison with IDH1− tumors ($p < 0.05$). The total choline/NAA (tCHO/NAA) ratio was also significantly decreased with in vivo MRS ($p = 0.04$) but not with the ex vivo HR-MAS method ($p = 0.13$) for IDH1+ tumors. Of note, glutamate (GLU) significantly decreased in IDH1+ tumors only with the ex vivo HR-MAS method ($p < 0.01$). 2-HG was undetectable by both modalities.

3.4 | Histopathological characterization of the *IDH1* mutant

No differential expression in proliferation was found between the IDH1+ and IDH1− tumors (54.47 ± 14.93 and 54.05 ± 2.92% respectively, $p = 0.58$), and a non-significant higher vascular density was observed for IDH1+ tumors (220.00 ± 38.10 versus 188.33 ± 13.74 vessels/mm^2, $p = 0.38$).

Received: | Accepted: Accepted paper

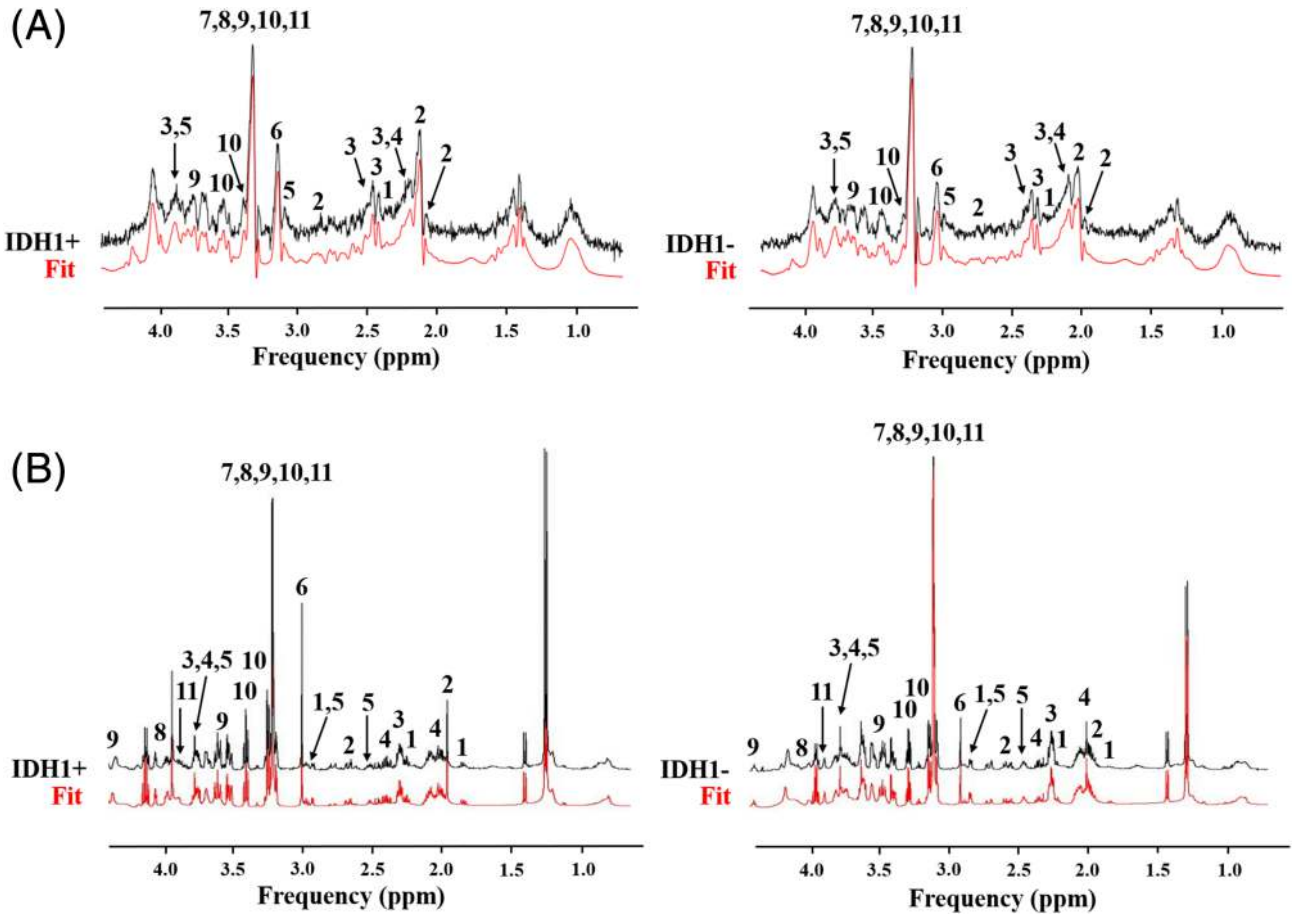

FIGURE 4 Spectra and fit of metabolic changes for *IDH1* mutation expression in human-derived glioblastomas according to their *IDH1* status with in vivo MRS (A) and ex vivo HR-MAS (B). Assignment: 1—gamma-aminobutyric acid (GABA), 2—NAA, 3—GLU, 4—glutamine (GLN), 5—GSH, 6—creatine + PCR, [7—choline, 8—phosphocholine, 9—glycerophosphocholine] (total choline), 10—TAU, 11—M-INS

When compared with healthy contralateral brain (<1% Ki-67 marker), tumors exhibited both higher proliferation ($p < 0.01$) and lower vascular density, with 390.00 ± 85.00 vessels/mm^2 for healthy tissue ($p < 0.01$). Representative sections are illustrated in Figure 5.

4 | DISCUSSION

In this multiparametric MRI and MRS study, the *IDH1* mutation, directly induced in the U87 cell lines, was associated with a higher vascular density and a lower permeability in brain tumors. These key features exhibited a statistical effect independent of tumor volume, and may represent the first steps toward the understanding of the pathophysiological mechanisms induced by this mutation. Moreover, a lower expression profile of metabolic aggressiveness was observed in both in vivo MRS and ex vivo HR-MAS for IDH1+ tumors, with, in particular, a lower tCho/NAA ratio and lower GSH level.

The biological effects of the *IDH1* mutation remain controversial with regard to the neoangiogenesis pathway. First, our MRI results showed that IDH1+ tumors exhibited higher vascular density, although this difference did not reach statistical significance in our histological analyses obtained in a small number of samples. This vascular density parameter was not investigated in previous studies exploring the effect of the overexpression of the *IDH1* mutation in gliomas.[27,28] Our results are nonetheless consistent with another multiparametric MRI study performed in humans with high-grade gliomas,[29] in which the microvessel type indicator was increased in IDH1+ tumors when compared with their IDH1− counterparts. The higher vascular density observed in the present study is likely associated with a better $CMRO_2$, although no difference was observed with our $CMRO_2$ measurements (3.16 ± 1.68% for IDH1+ versus 2.38 ± 1.09% for IDH1− tumors, $p = 0.25$). Irrespectively, this better $CMRO_2$ in IDH1+ tumors was also described in the study of Stadlbauer et al for high-grade gliomas.[29]

Second, a lower vessel permeability was observed herein in *IDH1*-mutant tumors. This permeability was studied through a semi-quantitative method, DCE-MRI, with the observation of a longer TTP and a lower contrast enhancement in *IDH1*-mutant tumors. This lower vessel

Received: | Accepted: Accepted paper

Metabolite	IDH1+ versus IDH1−	Significance (*p*)
Fused cell		
GABA	↗	0.01
GLN	=	0.14
GLU	=	0.83
GLX	=	0.21
GSH	↘	0.05
PCR	↗	0.03
TAU	↗	<0.01
M-INS	↗	0.01
Tcho	=	0.19
NAA	↗	0.01
tCHO/NAA	↘	0.04
Ex vivo HR-MAS		
GABA	=	0.22
GLN	=	0.49
GLU	↘	<0.01
GLX	↘	<0.01
GSH	↘	<0.01
PCR	↗	0.03
TAU	↗	0.03
M-INS	↗	0.02
tCHO	=	0.20
NAA	↗	0.05
tCHO/NAA	=	0.13

TABLE 1 Variations of main metabolic changes for *IDH1* expression in human-derived U87 glioblastoma cell lines with in vivo MRS and ex vivo HR-MAS. In bold, Mann-Whitney test with $p < 0.05$ significance

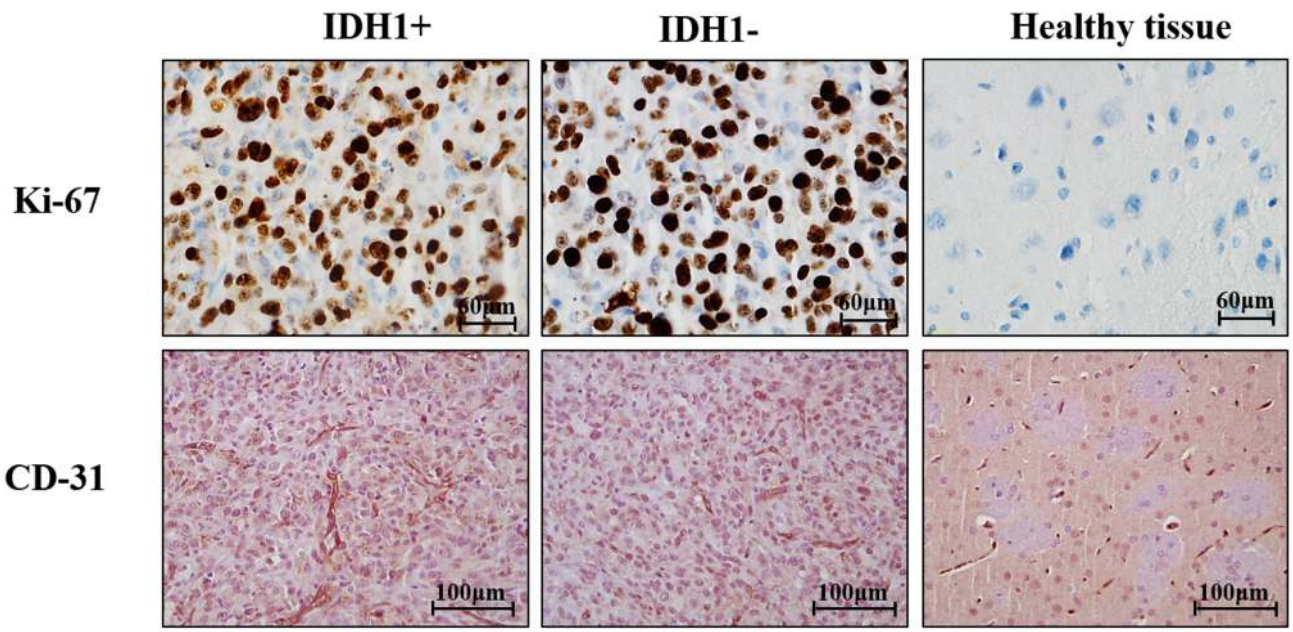

FIGURE 5 Representative sections of Ki67 proliferative index (upper panel, magnification ×40) and vessel density (lower panel, magnification ×20) in IDH1+ and IDH1− human-derived glioblastomas and in healthy rat brains. No differential expression in proliferation was found between IDH1+ and IDH1− tumors ($p = 0.58$). Quantification of vascular density using the CD31 marker showed a non-significant result observed for IDH1+ tumors ($p = 0.38$) but significantly lower vascularization in both glioblastomas lines compared with healthy brain tissue ($p < 0.01$)

permeability in *IDH1*-mutant tumors was also reported in the study by Lazovic et al, whereby IDH1+ tumors had slightly smaller areas of contrast enhancement compared with IDH1− gliomas.[27] In agreement with these results, Lu et al, in a study performed with DCE-MRI in human high-grade gliomas, also reported longer TTP for IDH1+ compared with IDH1− gliomas, suggestive of lower vascular permeability in IDH1+ tumors.[30]

The combination of a higher vascular density with a lower permeability in *IDH1*-mutant tumors represents the key features of the *IDH1* mutation status in the current study, since they provide valuable information independent of tumor volume. Indeed, as observed in the cluster-based approach, a different tumor signature was observed between IDH1+ and IDH1− tumors, which could prove useful in the assessment and monitoring of gliomas. Another crucial point is that, in contrast to other studies, the present results were obtained after the induction and not the overexpression of the *IDH1* mutation, ensuring that the observed differences are likely the result of the expression of this mutation. Given the above, we propose the hypothesis that the tumor vascular network of IDH1+ gliomas is more functional, with better vascular density and lower vessel permeability along with lower peripheral VSI features than those observed in IDH1− tumors, and thereby similar to the vasculature of healthy brain.

In addition, our study highlights a less aggressive metabolomic profile in IDH1+ tumors than in IDH1− tumors. This assessment was performed through a non-invasive in vivo MRS method, corroborated by ex vivo HR-MAS. It should be emphasized that in the current study neither in vivo MRS nor ex vivo HR-MAS was able to detect 2-HG. The most likely reason for this non-detection is the low concentration of 2-HG observed in our IDH1+ tumors (0.09 mM) compared with human gliomas where 2-HG reaches 2-9 mM,[31] with the NMR detection limit being in the millimolar range.[32] Based on the specifications of our provider (ATCC), we expected a much higher 2-HG concentration in IDH1+ tumors. However, our ex vivo analyses (western blot, immunohistochemistry and spectrophotometer absorbance, see Supporting Information) confirmed the expression of 2-HG in IDH1+ cell lines with a 2.25-fold increase compared with the IDH1− tumors. These results should be compared with other reported findings. For example, Ohka et al found a 1.33-fold increase in 2-HG in IDH1+ cell lines with a concentration nearing 2.00 mmol g^{-1} compared with 1.5 mmol g^{-1} in IDH1− cell lines. However, their model of U87 cell lines consisted of an overexpression of the *IDH1* mutation,[33] and was thus completely different from our current model using an original CRISP/Cas9 method, which has not yet been reported. Of particular note, our methodological expression of the *IDH1* mutation represents a more physiological setting and is closer to that observed in patient tumors.[34] Further compounding the issue is the fact that the main 2-HG resonances overlap with the NAA and GLU signals in the in vivo MRS spectra at the magnetic field used (4.7 T) and are thus difficult to observe.[35] However, it should be noted that GLU synthesis was shown to be impaired with a higher production of 2-HG in gliomas, which is in line with our observations of reduced GLU in ex vivo HR-MAS and reduced GSH for both in vivo MRS and ex vivo HR-MAS in IDH1+ tumors.[36] For these reasons, a number of MRS studies have recently proposed using metabolites other than 2-HG for *IDH1* mutation detection.[37,38] Although not all metabolites are detected with in vivo MRS due to the low magnetic field applied, our results are nevertheless in keeping with these previous studies by validating the concentration changes of other well known IDH1+-specific metabolites.[9,10,37,38] In particular, IDH1+ gliomas exhibited higher levels of NAA, TAU, PCR, and M-INS and a lower tCHO/NAA ratio, which are considered to be biomarkers of non-aggressive tumors.[39–43]

Analysis of our histological data did not reveal any significant difference in vascularization between IDH1+ and IDH1− gliomas. This could be explained by the fact that typical MR parameters measure functional vessels only, whereas histology stains all vessels (functional and non-functional). Indeed, MRI vascular parameter assessment required the injection of contrast agents and/or flowing blood. Therefore, only perfused vessels were quantified. This lack of difference may also be a result of the small number of samples used in our histological analysis, partly due to the fact that most post-sacrifice samples were used for HR-MAS. Ex vivo tests, performed in IDH1+ gliomas, have nonetheless reported that 2-HG production is responsible for the formation of new functional blood vessels.[44,45]

There are several limitations inherent to the current study. First, the tumor volumes observed in IDH1+ tumors were found to be almost half of those recorded for IDH1− tumors. Although the IDH1− tumors were first imaged with MRI, this difference could influence other functional MR parameters, such as those reflecting tumor vascularization. However, both vascular density and TTP were independent predictive factors of the *IDH1* mutation, irrespective of tumor volume. Second, the proposed animal model is based on human-derived glioblastoma cell lines, which are known to be poorly affected by the *IDH1* mutation.[46] The choice of using human-derived U87 glioblastoma cell lines grafted into our animal models is premised on the fact that high tumor growth rates, more adapted to achieving such preclinical analyses, are expected. In addition, in comparison with the less well characterized primary glioma stem-like cell lines, human-derived U87 glioblastoma cell lines are well defined and adapted to specifically study the effect of an induced mutation.

In summary, this study is the first to explore features induced directly by expression of the *IDH1* mutation in human-derived glioblastoma cell lines through a multiparametric MRI and MRS analysis. This mutation was found to lead to higher vascularity on MRI, a lower permeability, and a less aggressive metabolic profile in tumors. This non-invasive protocol tailored to the specific features of gliomas harboring the *IDH1* mutation could prove helpful for longitudinal treatment monitoring and prognostic studies, in particular when assessing *IDH1*-mutation-specific therapeutic strategies. Further analyses are needed to better assess the characteristics of this mutation through patient-derived models, involving lower-grade gliomas and multimodal imaging, including multi-tracer PET (positron emission tomography) imaging.

CONFLICTS OF INTEREST

The authors declare no conflict of interest.

DATA AVAILABILITY STATEMENT

Research data are not shared.

ORCID

Alexandra Clément https://orcid.org/0000-0003-2982-3070
Benjamin Lemasson https://orcid.org/0000-0003-0446-3531

REFERENCES

1. Louis DN, Perry A, Reifenberger G, et al. The 2016 World Health Organization Classification of Tumors of the Central Nervous System: a summary. *Acta Neuropathol*. 2016;131(6):803-820. https://doi.org/10.1007/s00401-016-1545-1
2. Qi ST, Yu L, Gui S, et al. *IDH* mutations predict longer survival and response to temozolomide in secondary glioblastoma. *Cancer Sci*. 2012;103(2):269-273. https://doi.org/10.1111/j.1349-7006.2011.02134.x
3. Tran AN, Lai A, Li S, et al. Increased sensitivity to radiochemotherapy in IDH1 mutant glioblastoma as demonstrated by serial quantitative MR volumetry. *Neuro-Oncology*. 2014;16(3):414-420. https://doi.org/10.1093/neuonc/not198
4. Dang L, White DW, Gross S, et al. Cancer-associated IDH1 mutations produce 2-hydroxyglutarate. *Nature*. 2010;465(7300):966–984. https://doi.org/10.1038/nature09132
5. Lu C, Ward PS, Kapoor GS, et al. IDH mutation impairs histone demethylation and results in a block to cell differentiation. *Nature*. 2012;483(7390):474-478. https://doi.org/10.1038/nature10860
6. Xu W, Yang H, Liu Y, et al. Oncometabolite 2-hydroxyglutarate is a competitive inhibitor of α-ketoglutarate-dependent dioxygenases. *Cancer Cell*. 2011;19(1):17-30. https://doi.org/10.1016/j.ccr.2010.12.014
7. Yang H, Ye D, Guan K-L, Xiong Y. IDH1 and IDH2 mutations in tumorigenesis: mechanistic insights and clinical perspectives. *Clin Cancer Res*. 2012;18(20):5562-5571. https://doi.org/10.1158/1078-0432.CCR-12-1773
8. Masui K, Cavenee WK, Mischel PS. Cancer metabolism as a central driving force of glioma pathogenesis. *Brain Tumor Pathol*. 2016;33(3):161-168. https://doi.org/10.1007/s10014-016-0265-5
9. Izquierdo-Garcia JL, Viswanath P, Eriksson P, et al. Metabolic reprogramming in mutant IDH1 glioma cells. *PLoS ONE*. 2015;10(2):e0118781. https://doi.org/10.1371/journal.pone.0118781
10. Reitman ZJ, Jin G, Karoly ED, et al. Profiling the effects of isocitrate dehydrogenase 1 and 2 mutations on the cellular metabolome. *Proc Natl Acad Sci U S A*. 2011;108(8):3270-3275. https://doi.org/10.1073/pnas.1019393108
11. Houillier C, Wang X, Kaloshi G, et al. IDH1 or IDH2 mutations predict longer survival and response to temozolomide in low-grade gliomas. *Neurology*. 2010;75(17):1560-1566. https://doi.org/10.1212/WNL.0b013e3181f96282
12. Natsumeda M, Motohashi K, Igarashi H, et al. Reliable diagnosis of IDH-mutant glioblastoma by 2-hydroxyglutarate detection: a study by 3-T magnetic resonance spectroscopy. *Neurosurg Rev*. 2018;41(2):641-647. https://doi.org/10.1007/s10143-017-0908-y
13. Leather T, Jenkinson MD, Das K, Poptani H. Magnetic resonance spectroscopy for detection of 2-hydroxyglutarate as a biomarker for IDH mutation in gliomas. *Metabolites*. 2017;7(2):29–45. https://doi.org/10.3390/metabo7020029
14. Crisi G, Filice S, Michiara M, Crafa P, Lana S. 2-hydroxyglutarate detection by short echo time magnetic resonance spectroscopy in routine imaging study of brain glioma at 3.0 T. *J Comput Assist Tomogr*. 2018;42(3):469-474. https://doi.org/10.1097/RCT.0000000000000705
15. Natsumeda M, Igarashi H, Nomura T, et al. Accumulation of 2-hydroxyglutarate in gliomas correlates with survival: a study by 3.0-tesla magnetic resonance spectroscopy. *Acta Neuropathol Commun*. 2014;2:158-165. https://doi.org/10.1186/s40478-014-0158-y
16. Emir UE, Larkin SJ, de Pennington N, et al. Noninvasive quantification of 2-hydroxyglutarate in human gliomas with IDH1 and IDH2 mutations. *Cancer Res*. 2016;76(1):43-49. https://doi.org/10.1158/0008-5472.CAN-15-0934
17. Cong L, Ran FA, Cox D, et al. Multiplex genome engineering using CRISPR/Cas systems. *Science*. 2013;339(6121):819-823. https://doi.org/10.1126/science.1231143
18. Toussaint M, Pinel S, Auger F, et al. Proton MR spectroscopy and diffusion MR imaging monitoring to predict tumor response to interstitial photodynamic therapy for glioblastoma. *Theranostics*. 2017;7(2):436-451. https://doi.org/10.7150/thno.17218
19. Kobayashi N, Allen N, Clendenon NR, Ko LW. An improved rat brain-tumor model. *J Neurosurg*. 1980;53(6):808-815. https://doi.org/10.3171/jns.1980.53.6.0808
20. Lemasson B, Christen T, Tizon X, et al. Assessment of multiparametric MRI in a human glioma model to monitor cytotoxic and anti-angiogenic drug effects. *NMR Biomed*. 2011;24(5):473-482. https://doi.org/10.1002/nbm.1611
21. Bottomley PA. Spatial localization in NMR spectroscopy in vivo. *Ann N Y Acad Sci*. 1987;508(1 Physiological):333-348. https://doi.org/10.1111/j.1749-6632.1987.tb32915.x
22. Tkác I, Starcuk Z, Choi IY, Gruetter R. In vivo ^{1}H NMR spectroscopy of rat brain at 1 ms echo time. *Magn Reson Med*. 1999;41(4):649-656. https://doi.org/10.1002/(sici)1522-2594(199904)41:4%3C649::aid-mrm2%3E3.0.co;2-g
23. Kanayama S, Kuhara S, Satoh K. In vivo rapid magnetic field measurement and shimming using single scan differential phase mapping. *Magn Reson Med*. 1996;36(4):637-642. https://doi.org/10.1002/mrm.1910360421
24. Čuperlović-Culf M, Barnett DA, Culf AS, Chute I. Cell culture metabolomics: applications and future directions. *Drug Discov Today*. 2010;15(15-16):610-621. https://doi.org/10.1016/j.drudis.2010.06.012
25. Pouget C, Hergalant S, Lardenois E, et al. Ki-67 and MCM6 labelling indices are correlated with overall survival in anaplastic oligodendroglioma, *IDH1*-mutant and 1p/19q-codeleted: a multicenter study from the French POLA network [published online ahead of print September 27, 2019. *Brain Pathol*. 2020;30(3):465–478. https://doi.org/10.1111/bpa.12788
26. Baudry J-P, Maugis C, Michel B. Slope heuristics: overview and implementation. *Stat Comput*. 2012;22(2):455-470. https://doi.org/10.1007/s11222-011-9236-1
27. Lazovic J, Soto H, Piccioni D, et al. Detection of 2-hydroxyglutaric acid in vivo by proton magnetic resonance spectroscopy in U87 glioma cells overexpressing isocitrate dehydrogenase-1 mutation. *Neuro-Oncology*. 2012;14(12):1465-1472. https://doi.org/10.1093/neuonc/nos258

28. Chaumeil MM, Larson PEZ, Yoshihara HAI, et al. Non-invasive in vivo assessment of IDH1 mutational status in glioma. *Nat Commun*. 2013;4(1): 2429-2441. https://doi.org/10.1038/ncomms3429
29. Stadlbauer A, Zimmermann M, Kitzwögerer M, et al. MR imaging-derived oxygen metabolism and neovascularization characterization for grading and *IDH* gene mutation detection of gliomas. *Radiology*. 2017;283(3):799-809. https://doi.org/10.1148/radiol.2016161422
30. Lu HT, Xing W, Zhang YW, Qin HP, Wu RH, Ding JL. The value of DCE-MRI in predicting IDH gene mutation of high-grade gliomas. 2019;99(39): 3105-3109. https://doi.org/10.3760/cma.j.issn.0376-2491.2019.39.013
31. Choi C, Ganji SK, DeBerardinis RJ, et al. 2-hydroxyglutarate detection by magnetic resonance spectroscopy in IDH-mutated patients with gliomas. *Nat Med*. 2012;18(4):624-629. https://doi.org/10.1038/nm.2682
32. Bertolino N, Marchionni C, Ghielmetti F, et al. Accuracy of 2-hydroxyglutarate quantification by short-echo proton-MRS at 3 T: a phantom study. *Phys Medica*. 2014;30(6):702-707. https://doi.org/10.1016/j.ejmp.2014.03.002
33. Ohka F, Ito M, Ranjit M, et al. Quantitative metabolome analysis profiles activation of glutaminolysis in glioma with IDH1 mutation. *Tumour Biol*. 2014; 35(6):5911-5920. https://doi.org/10.1007/s13277-014-1784-5
34. Bumes E, Wirtz F-P, Fellner C, et al. Non-invasive prediction of *IDH* mutation in patients with glioma WHO II/III/IV based on F-18-FET PET-guided in vivo ^{1}H-magnetic resonance spectroscopy and machine learning. *Cancer*. 2020;12(11):3406–3421. https://doi.org/10.3390/cancers12113406
35. Tiwari V, Mashimo T, An Z, et al. In vivo MRS measurement of 2-hydroxyglutarate in patient-derived IDH-mutant xenograft mouse models versus glioma patients. *Magn Reson Med*. 2020;84(3):1152-1160. https://doi.org/10.1002/mrm.28183
36. McBrayer SK, Mayers JR, DiNatale GJ, et al. Transaminase inhibition by 2-hydroxyglutarate impairs glutamate biosynthesis and redox homeostasis in glioma. *Cell*. 2018;175(1):101-116.e25. https://doi.org/10.1016/j.cell.2018.08.038
37. Pope WB, Prins RM, Albert Thomas M, et al. Non-invasive detection of 2-hydroxyglutarate and other metabolites in IDH1 mutant glioma patients using magnetic resonance spectroscopy. *J Neuro-Oncol*. 2012;107(1):197-205. https://doi.org/10.1007/s11060-011-0737-8
38. Nagashima H, Tanaka K, Sasayama T, et al. Diagnostic value of glutamate with 2-hydroxyglutarate in magnetic resonance spectroscopy for IDH1 mutant glioma. *Neuro-Oncology*. 2016;18(11):1559-1568. https://doi.org/10.1093/neuonc/now090
39. Gómez-Angelats M, Cidlowski JA. Cell volume control and signal transduction in apoptosis. *Toxicol Pathol*. 2002;30(5):541-551. https://doi.org/10.1080/01926230290105820
40. Gandía-González ML, Cerdán S, Barrios L, et al. Assessment of overall survival in glioma patients as predicted by metabolomic criteria. *Front Oncol*. 2019;9:328-339. https://doi.org/10.3389/fonc.2019.00328
41. Sontheimer H. A role for glutamate in growth and invasion of primary brain tumors. *J Neurochem*. 2008;105(2):287-295. https://doi.org/10.1111/j.1471-4159.2008.05301.x
42. Guo J, Yao C, Chen H, et al. The relationship between Cho/NAA and glioma metabolism: implementation for margin delineation of cerebral gliomas. *Acta Neurochir*. 2012;154(8):1361-1370, discussion 1370. https://doi.org/10.1007/s00701-012-1418-x
43. Jalbert LE, Elkhaled A, Phillips JJ, et al. Metabolic profiling of IDH mutation and malignant progression in infiltrating glioma. *Sci Rep*. 2017;7(1): 44792–44802. https://doi.org/10.1038/srep44792
44. Seok J, Yoon S, Lee S, Jung JH, Lee YM. The oncometabolite d-2-hydroxyglutarate induces angiogenic activity through the vascular endothelial growth factor receptor 2 signaling pathway. *Int J Oncol*. 2019;54(2):753-763. https://doi.org/10.3892/ijo.2018.4649
45. Mao MJ, Leonardi DE. Vascular-endothelial response to IDH1 mutant fibrosarcoma secretome and metabolite: implications on cancer microenvironment. *Am J Cancer Res*. 2019;9(1):122-133.
46. Jiang H, Cui Y, Wang J, Lin S. Impact of epidemiological characteristics of supratentorial gliomas in adults brought about by the 2016 World Health Organization classification of tumors of the central nervous system. *Oncotarget*. 2017;8(12):20354-20361. https://doi.org/10.18632/oncotarget.13555